3-2015

On the use of drift echoes to characterize on-orbit sensor discrepancies

T. P. O'Brien
Aerospace Corporation

S. Claudepierre
Aerospace Corporation

M. Looper
Aerospace Corporation

J. B. Blake
Aerospace Corporation

J. F. Fennell
Aerospce Corporation

See next page for additional authors

Recommended Citation

T. P. O'Brien, S. G. Claudepierre, M. D. Looper, J. B. Blake, J. F. Fennell, J. H. Clemmons, J. L. Roeder, S. G. Kanekal, J. W. Manweiler, D. G. Mitchell, M. Gkioulidou, L. J. Lanzerotti, H. E. Spence, G. D. Reeves, and D. N. Baker, 'On the use of drift echoes to characterize on-orbit sensor discrepancies', Journal of Geophysical Research: Space Physics, vol. 120, no. 3, pp. 2076–2087, Mar. 2015.

AGU PUBLICATIONS

JGR

Journal of Geophysical Research: Space Physics

RESEARCH ARTICLE
10.1002/2014JA020859

Special Section:
New perspectives on Earth's radiation belt regions from the prime mission of the Van Allen Probes

On the use of drift echoes to characterize on-orbit sensor discrepancies

T. P. O'Brien[1], S. G. Claudepierre[1], M. D. Looper[1], J. B. Blake[1], J. F. Fennell[1], J. H. Clemmons[1], J. L. Roeder[1], S. G. Kanekal[2], J. W. Manweiler[3], D. G. Mitchell[4], M. Gkioulidou[4], L. J. Lanzerotti[5], H. E. Spence[6], G. D. Reeves[7], and D. N. Baker[8]

[1]Space Sciences Department, The Aerospace Corporation, El Segundo, California, USA, [2]Goddard Space Flight Center, Greenbelt, Maryland, USA, [3]Fundamental Technologies LLC, Lawrence, Kanas, USA, [4]Space Department, Johns Hopkins University Applied Physics Laboratory, Laurel, Maryland, USA, [5]Center for Solar Terrestrial Research, Department of Physics, New Jersey Institute of Technology, Newark, New Jersey, USA, [6]Institute for the Study of Earth, Oceans, and Space, University of New Hampshire, Durham, New Hampshire, USA, [7]Space and Atmospheric Sciences Group, Los Alamos National Laboratory, Los Alamos, New Mexico, USA, [8]Laboratory for Atmospheric and Space Physics, University of Colorado Boulder, Boulder, Colorado, USA

Abstract We describe a method for using drift echo signatures in on-orbit data to resolve discrepancies between different measurements of particle flux. The drift period has a well-defined energy dependence, which gives rise to time dispersion of the echoes. The dispersion can then be used to determine the effective energy for one or more channels given each channel's drift period and the known energy for a reference channel. We demonstrate this technique on multiple instruments from the Van Allen Probes mission. Drift echoes are only easily observed at high energies (100 s keV to multiple MeV), where several drift periods occur before the observing satellite has moved on or the global magnetic conditions have changed. We describe a first-order correction for spacecraft motion. The drift echo technique has provided a significant clue in resolving substantial flux discrepancies between two instruments measuring fluxes near 2 MeV.

Key Points:
- The drift echo period in a static magnetic field is a function of particle energy
- All channels on the same spacecraft must give consistent energy versus drift period
- Knowing only one channel's energy, it is possible to infer all others' energies

Correspondence to:
T. P. O'Brien,
paul.obrien@aero.org

Citation:
O'Brien, T. P., et al. (2015), On the use of drift echoes to characterize on-orbit sensor discrepancies, *J. Geophys. Res. Space Physics*, *120*, 2076–2087, doi:10.1002/2014JA020859.

Received 19 NOV 2014
Accepted 29 JAN 2015
Accepted article online 4 FEB 2015
Published online 3 MAR 2015

1. Introduction

Ideally, preflight calibration of particle sensors would leave no doubt as to how to convert an observed count rate into a flux. In practice, however, it is common to find two instruments on the same spacecraft reporting mismatched fluxes at the same energy. This happens for a variety of reasons, the most common of which is the necessity of deriving flux at a single energy from a count rate that convolves the true spectrum with a possibly complex energy response. This is especially problematic when, as is often the case, spacecraft resource limitations lead to wide energy channels. The preflight simplifying assumptions (e.g., bowtie analysis [*Selesnick and Blake,* 2000; *Baker et al.,* 2012]) do not always adequately address the realities observed on orbit, especially when a new sensor confronts a new radiation environment that was largely unknown prior to launch.

Several recent papers have addressed the issue of cross-calibration factors [e.g., *Friedel et al.,* 2005; *Sandberg et al.,* 2014; *Kellerman et al.,* 2014]. In these papers, the method is usually to adjust the flux of one sensor to match the flux of a reference sensor using a multiplicative scale factor. This type of correction assumes that the effective energy of the channel is known, while something about its flux conversion factor (i.e., geometric factor, efficiency, and energy bandwidth) is different on orbit from what was originally assumed. The analysis we present below takes an orthogonal approach: using electron drift echoes measured by several Van Allen Probes instruments, we will examine the most appropriate energy assignment for a channel independent of whether the flux conversion factor is correct.

Electron drift echoes were first identified in an instrument's electron differential energy channels by *Lanzerotti et al.* [1967] from measurements made on the geosynchronous communications test satellite ATS-1. Subsequently, following a sudden commencement event in November 1968, *Lanzerotti et al.* [1971] identified proton drift echoes using the same instrument. Electron drift echoes can sometimes also be identified in integral electron channels (e.g., in the March 1991 shock event [*Blake et al.,* 1992]). Our emphasis in this work will be on the use of drift echoes to verify or falsify the energy channel assignments for differential energy channels. Specifically, we aim to resolve a large flux discrepancy seen near 2 MeV between the high unit of the Magnetic Electron Ion Spectrometer (MagEIS) [*Blake et al.,* 2013] and the Relativistic Electron-Proton

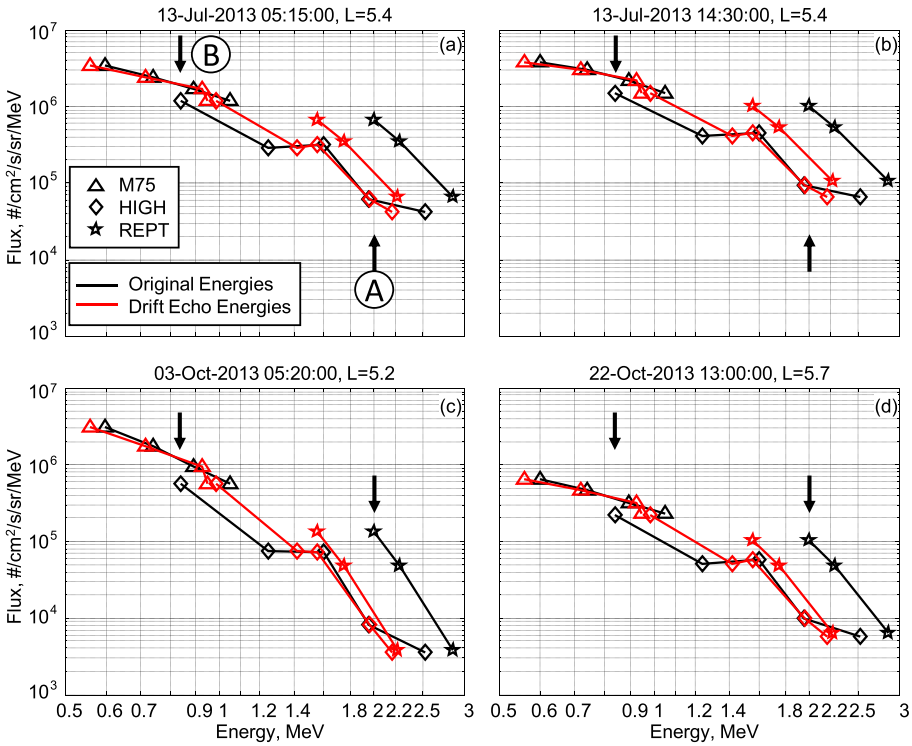

Figure 1. Four example energy spectra from MagEIS and REPT for ~0.5–3 MeV. M75 is the MagEIS medium 75 unit, and HIGH is MagEIS high. Black indicates observations plotted at original (release 2) energy channel labels; red indicates the same fluxes shifted horizontally and plotted at energy values determined from the drift echo analysis described in the text. The spectrum from each sensor is presented separately using different symbols. Marker A indicates the large discrepancy in flux between REPT and MagEIS high near 2 MeV using the original energies, and marker B indicates the inconsistency between MagEIS medium and high units around 0.9 MeV.

Telescope (REPT) [*Baker et al.,* 2012] on board NASA's Van Allen Probes (launched as Radiation Belt Storm Probes (RBSP)). Figure 1 shows four different spectra from 0.5 to 3 MeV using data from the MagEIS medium (M75), MagEIS high, and REPT sensors on the RBSP-B spacecraft. Black traces show the spectrum using the original energies. Near 2 MeV, REPT fluxes are as much as a factor of 10 higher than MagEIS high fluxes in the currently publicly available data release (release 2 and prior). Near 0.9 MeV, MagEIS medium fluxes are about a factor of 2 higher than MagEIS high fluxes. As noted earlier, REPT flux and energy bin values are dependent upon assumption of spectral shape and parameters used in the bowtie analysis. The flattening observed near 1.4 MeV is often seen in the outer zone data from MagEIS and REPT.

We will work through the analysis that leads to the red traces in Figure 1, which have simply moved each point horizontally to a new energy determined by drift echo analysis (i.e., we have not adjusted the flux values in the vertical direction). In all cases the new energies bring the spectrum into better agreement among the instruments. We will conclude by comparing the drift echo energies to a revised set of energies for each sensor, that revision being based on recent analysis of each sensor's energy response.

2. Satellite Data

We will examine electron fluxes from several different instruments on the *B* spacecraft of NASA's Van Allen Probes mission. There are two probes, instrumented identically in low inclination, ~9 h elliptical orbits, with a low-altitude perigee and an apogee about 5.8 R_E from the center of the Earth. The probes spin at 5.5 rpm with an axis roughly pointing toward the Sun. The flux discrepancies we have shown in Figure 1 are present on both spacecraft, so it is only necessary to analyze one to demonstrate the drift echo technique.

The first set of instruments in our study come from the Energetic Particle, Composition, and Thermal Plasma (ECT) suite [*Spence et al.,* 2013]: MagEIS and REPT. The MagEIS instrument consists of four separate units: a low, two medium, and a high unit. We use level two (release 2, v3.1.0) spin-averaged data with a time

resolution of 11 s. The MagEIS low unit has eight energy channels measuring electrons from about 20 to 200 keV and was only used in preliminary versions of this study. The two medium units are oriented at different angles to the spacecraft spin axis to improve total angular coverage and are denoted M35 and M75 for 35° and 75° from the spin axis, respectively (the other units view 75° from the spin axis). The two medium units have eight energy channels measuring electrons from about 146 to 1040 keV, and we used the top four channels (~0.6–1.1 MeV). The high unit has seven energy channels from about 1 to 4 MeV, and we use the first five channels (up to ~3 MeV). The REPT instrument measures electrons in 12 channels from about 1.8 to 18 MeV. We use level two (release 2, v3.1.0) spin-averaged data at a time resolution of 11 s. We use the first three REPT channels (up to ~3 MeV). We note that in the forthcoming release 3, the flux discrepancies between MagEIS and REPT are dramatically reduced through revision to the energy channel labels and flux conversions (see below, section 6).

The final instrument in our study is the Radiation Belt Storm Probes Ion Composition Experiment (RBSPICE) [*Mitchell et al.,* 2013], which measures electrons from about 25 keV to 1 MeV in up to 64 energy channels. We use RBSPICE for additional verification of the method and channel energies. We use level three (v1.1.7-02) high-energy resolution data with a cadence of 109 s. We note that a 1 MeV electron at $L = 4.5–6$ in a dipole has a drift period longer than 650 s. Thus, RBSPICE time resolution is more than adequate for detecting any drift echoes we are likely to encounter, although its resolution of the estimated drift period for individual events will be as wide as 17%. The data are 10-spin averages in multiple spin phase sectors for multiple telescopes. To compute a spin average, we average over all spin sectors and five of the six telescopes (the last telescope is a background sensor and was not used). Because our analysis includes a substantial manual verification step, we only use three RBSPICE channels: 53, 58, and 63 (~0.5–1 MeV), which overlap with the MagEIS medium-energy range.

In preliminary studies preparing for this article, we used a larger set of energy channels, spanning from about 300 keV to 5 MeV. However, ultimately, we used the reduced set because they could be analyzed with high confidence by studying only four drift echo events. In the preliminary study, we manually identified 17 drift echo events from July to October 2013. Of these events, we selected four as the best demonstration of the technique: drift echoes were present in each event in nearly all energy channels from 0.5 to 3 MeV involving both MagEIS medium units, MagEIS high, REPT, and RBSPICE. We note that in the original 17 events, we found drift echoes above and below the 0.5 to 3 MeV range, but we have omitted them here in order to keep the demonstration as simple and clear as possible. Two events occur on 13 July 2013 near $L \sim 6$, one at about 0630, and the other at about 1630 UT. The other two events occur near $L \sim 4.5$ on 3 and 22 October 2013 near midnight and 0900 UT, respectively. The spectra in Figure 1 were chosen at times near, but not within, these drift echo events. We note that MagEIS High on the *B* spacecraft was undergoing efficiency tuning during July 2013, but that affects the flux conversion factor, not the shape or location of the energy response.

All the instruments in this study are susceptible to background. For MagEIS, we were able to confirm that the background was not significant in our study by examining preliminary background-corrected data (see S. G. Claudepierre et al., A background correction algorithm for Van Allen Probes MagEIS electron flux measurements, submitted to *Journal of Geophysical Research*, doi:10.1002/2014JA020876, 2014). For RBSPICE, we determined that the study events are largely free of background by comparing to MagEIS medium. For REPT, we determined that the fluxes were well above background by examining the *L* profile. In any case, background signatures are typically broadband and would not, therefore, exhibit strong drift echoes.

We note that different instruments and authors adopt different conventions for the energy channel number. We have adopted a zero-based system for all sensors. The MagEIS low and medium units have background channel zero, so that our channel numbers correspond to those of *Blake et al.* [2013] for the low and medium units. The MagEIS high unit has a programmable set of channels, and no dedicated background channel, so there is no correspondence between our channel numbers for the high unit and those of *Blake et al.* [2013]. *Baker et al.* [2012] use a one-based list of channels for REPT, so our numbers are lower by one. RBSPICE [*Mitchell et al.,* 2013] uses zero-based channel numbers, so our numbers match. The last MagEIS medium channel is M35-P8 or M75-P8, the first MagEIS high channel is HIGH-P0, the first REPT channel is REPT-P0, and the last RBSPICE channel is denoted RBSPICE-P63. The full set of 19 channels can be found in Table 1. Next we will explore the mathematical relationship between drift period and energy.

Table 1. Energy Channels and Drift Echo Results

Channel	Original Energy (MeV)	Drift Echo Energy (MeV)	% Difference Versus Original	Drift Echo % Error (2σ)	Number of Events	Revised Energy (MeV)
RBSPICE-P53	0.512	0.560	+9.43	27.5	3	0.512
M35-P5	0.594	0.587	−1.22	27.6	3	0.573
M75-P5	0.600	0.578	−3.66	27.5	3	0.573
RBSPICE-P58	0.692	0.812	+17.3	27.4	4	0.692
M35-P6	0.736	0.745	+1.20	27.4	4	0.719
M75-P6	0.743	0.743	0	26.0	4	0.719
HIGH-P0	0.841	1.02	+20.9	27.5	3	1.06
M35-P7	0.878	0.940	+7.06	27.3	4	0.874
M75-P7	0.892	0.953	+6.88	27.3	4	0.874
RBSPICE-P63	0.939	1.12	+19.3	27.4	3	0.939
M75-P8	1.05	0.98	−6.89	27.3	4	1.03
M35-P8	1.05	1.03	−1.89	27.2	4	1.03
HIGH-P1	1.25	1.46	+17.5	26.8	4	1.58
HIGH-P2	1.60	1.60	+0.212	26.6	4	1.73
HIGH-P3	1.96	2.03	+3.61	26.4	3	2.23
REPT-P0	2.00	1.60	−19.9	26.6	4	1.80
REPT-P1	2.25	1.81	−19.8	26.4	4	2.10
HIGH-P4	2.52	2.24	−11.2	26.0	4	2.56
REPT-P2	2.85	2.30	−19.4	26.0	4	2.60

3. Drift Period Formulation

The dipole drift period T_d is given by [see, e.g., *Schulz and Lanzerotti*, 1974, p. 21]:

$$\frac{2\pi}{T_d} = \Omega_d = \hat{\omega}(\alpha_{\mathrm{eq}}) L \frac{\gamma^2 - 1}{\gamma} = \hat{\omega}(\alpha_{\mathrm{eq}}) L \frac{E(E+2)}{E+1}, \tag{1}$$

where Ω_d represents the angular drift frequency, L is the drift shell, γ is the relativistic factor, and $\hat{\omega}(\alpha_{\mathrm{eq}})$ carries the dependence on equatorial pitch angle. (In a dipole, the L and angle dependence are multiplicatively separable.) We have used the relation $\gamma = E + 1$ for kinetic energy E in units of the rest mass equivalent energy (0.511 MeV). While the L and pitch angle dependences are functions of the global magnetic field, the energy dependence through γ is independent of the details of the magnetic field. For particles of the same species, with sufficient energy to neglect the electric field, their guiding-center trajectories can be uniquely defined by the modified second and third invariants K and L^*, which are both independent of energy. Thus, the energy affects *only* the drift rate, and that effect is multiplicatively separable from the dependence on the details of the global magnetic field configuration. The drift period T in *any* quasi-static field depends on energy as

$$T \propto \frac{E+1}{E(E+2)}. \tag{2}$$

To compute the drift echo period, we have experimented with using pitch angle resolved fluxes, but we have found that the improved counting statistics for spin-averaged fluxes allow us to extend the analysis to higher energies. Therefore, we replace $\hat{\omega}(\alpha_{\mathrm{eq}})$ in (1) with an average value $\overline{\omega}$. Using the formulae from *Schulz and Lanzerotti* [1974, p. 21], it can be shown that in a dipole field, for a vehicle spinning perpendicular to the magnetic field, the spin-averaged drift period differs only by about 10% for a steep $\sin^5(\alpha)$ angular distribution versus an isotropic distribution. Thus, any energy dependence of the angular distribution is not likely to have much effect on the rest of our analysis.

If the drift echo phases are all roughly synchronized by some initial impulse, then a moving spacecraft will see the following phase structure in time:

$$\varphi = \Omega_d(t) t \approx \overline{\omega} L(t) \frac{E(E+2)}{E+1} t. \tag{3}$$

If we then think of the correlation between an observed flux time series and itself lagged Δt in time, then the correlation will peak when

$$\Delta\varphi = \varphi(t + \Delta t) - \varphi(t) = 2\pi n \tag{4}$$

for any integer n.

The autocorrelation is strongest at $n = 1$ before the drift echo begins to wash out due to energy and pitch angle drift dispersion within the channel, spacecraft motion, or other magnetospheric processes disrupting the drift echo. Therefore, we will identify the observed drift period T as the time of peak correlation and relate it to its exact energy and approximate L dependence as

$$T \approx \frac{2\pi}{\overline{\omega} L_T} \frac{E+1}{E(E+2)}. \tag{5}$$

We have defined L_T as an effective L representing the midpoint L of the points used in the correlation at time lag T. If we observe the drift period for two different energy channels, then the ratio of those drift periods is as follows:

$$\frac{T_2}{T_1} \approx \frac{L_1}{L_2} \frac{\left(\frac{E_2+1}{E_2(E_2+2)}\right)}{\left(\frac{E_1+1}{E_1(E_1+2)}\right)}. \tag{6}$$

The ratio of energy factors is then

$$\frac{\left(\frac{E_2+1}{E_2(E_2+2)}\right)}{\left(\frac{E_1+1}{E_1(E_1+2)}\right)} \approx \frac{T_2 L_2}{T_1 L_1}. \tag{7}$$

We can, therefore, infer the energy of one channel given the TL ratio of drift periods and effective L values between that channel and a reference channel with known energy. We note that for a spacecraft nearly stationary during the period of observation, the L_2/L_1 ratio approaches unity, leaving an expression that is true in any magnetic field capable of trapping charged particles in adiabatic motion. We use the L dependence for a dipole-like field only to develop a first-order correction for variation of drift period with spacecraft motion, not to compute the period itself. We will use the ratio in (7) to estimate the energies of many electron flux channels relative to a reference channel of known energy.

4. Time Series Analysis

For the four events we selected for detailed analysis, we have grouped the energy channels together based on similarity of apparent drift echo periods. Within each group, we manually select the start and end time of the drift echo interval. The start and end times are energy dependent, so they also occur at slightly different effective L. Once we have the start and end times selected, we can make the set of plots for each channel group composing each row of Figure 2. Figures 2a, 2d, 2g, 2j, 2m, 2p, 2s, and 2v show the original flux time series within the selected time limits. We note that the flux levels do not always match (e.g., Figures 2d, 2p, and 2s), even if the drift echoes appear to be synchronized. This indicates a possible discrepancy in the flux conversion factor or the presence of background (although for these events, we believe background has been ruled out, except for RBSPICE-P58, which shows some background after 1:00 that is removed during detrending).

Figures 2b, 2e, 2h, 2k, 2n, 2q, 2t, and 2w show the detrended flux. For each channel, we estimate the trend by fitting the log flux to a fifth-order polynomial in time. We then divide the flux by this trend. For panels with multiple channels in them, we see that the detrended fluxes often agree very well in the phase and amplitude of the echo signature (again, Figures 2d, 2p, and 2s are excellent examples).

Next we compute the autocorrelation as a function of lag (Figures 2c, 2f, 2i, 2l, 2o, 2r, 2u, and 2x) for the detrended time series. Given the nominal energy for each channel in the panel and the effective L shell of the interval, we can compute the dipole drift period T_d for 45° equatorial pitch angle particles (colored vertical dashed lines). We use McIlwain L in the Olson-Pfitzer Quiet field model [*Olson and Pfitzer*, 1977]. We manually identify the drift period as the peak (symbols) in the autocorrelation function that is nearest the dipole T_d. Using this procedure, we obtain a drift period from the autocorrelation of the detrended flux for each energy channel. In this event, every channel has a clear drift echo. That is not the case in the other three events (not shown).

To distinguish drift echoes from drift resonances, in which all channels oscillate at the same frequency [e.g., *Claudepierre et al.*, 2013], we confirm that the peak autocorrelation is, in fact, energy dependent. In Figure 2 we

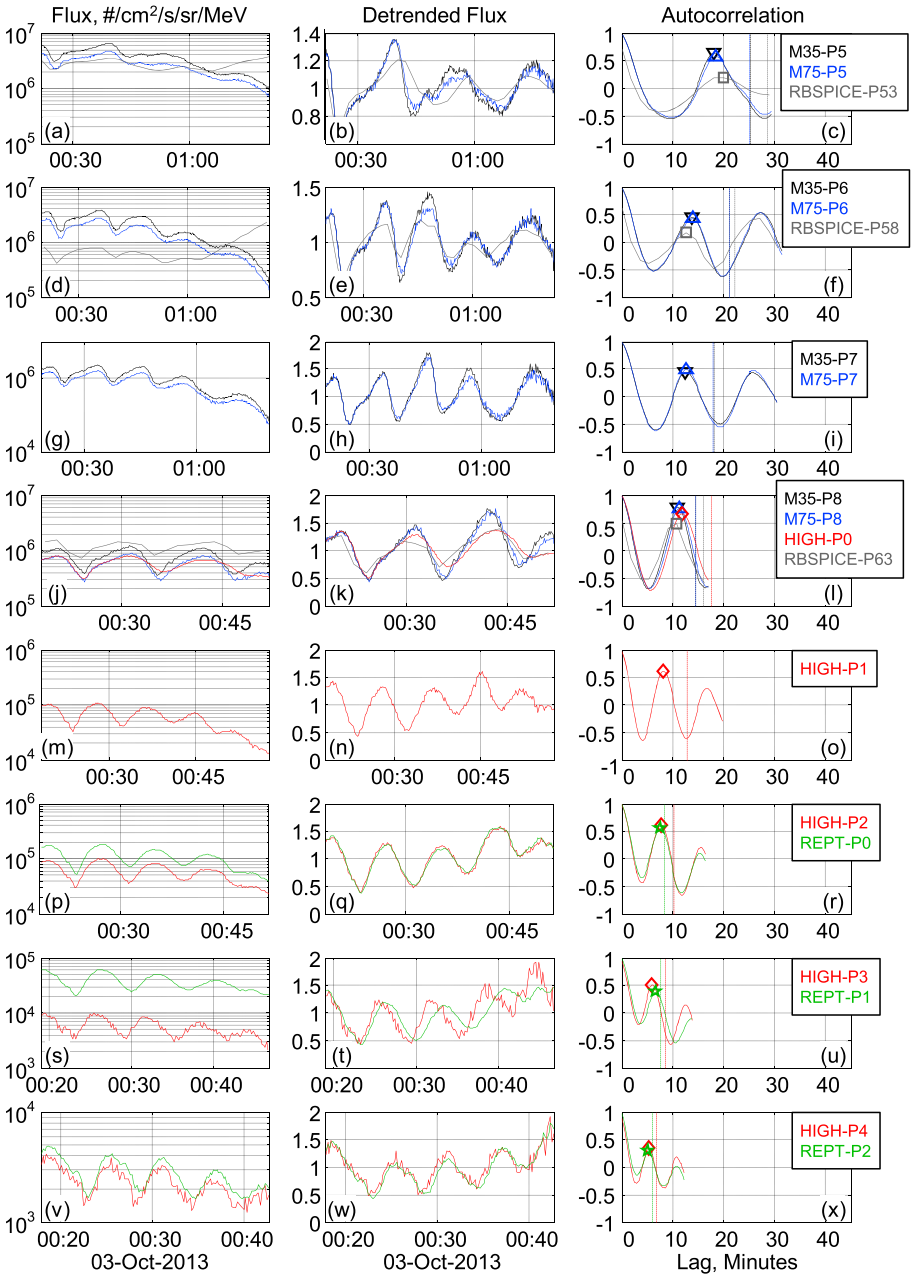

Figure 2. Time series analysis of the 3 October 2013 drift echo event. (a, d, g, j, m, p, s, and v) Flux time series. (b, e, h, k, n, q, t, and w) Detrended flux time series. (c, f, i, l, o, r, u, and x) Autocorrelation versus time lag. Colored traces indicate different energy channels from different sensors. M35 and M75 refer to the two MagEIS medium units. HIGH is the MagEIS high sensor. Colored vertical dashed lines in Figures 2c, 2f, 2i, 2l, 2o, 2r, 2u, and 2x provide the dipole drift period for the channel with the corresponding color. Symbols in Figures 2c, 2f, 2i, 2l, 2o, 2r, 2u, and 2x indicate the manually selected drift period at peak autocorrelation for each energy channel.

see a clear trend of longer drift periods at top (lower energies) to shorter drift periods at bottom (higher energies). Also, in this particular event at $L \sim 4.5$ the drift periods are all slightly shorter than the dipole values.

We have performed this manual analysis for all four drift echo events and all 19 channels. We ended up with 70 different drift period estimates rather than 76 because some channels exhibited drift echoes in only three of the four events. Figure 3 shows MagEIS-P2 and REPT-P0 for all four events. Figures 3g–3i are repeated from Figures 2p–2r. The fluxes of REPT-P0 are consistently higher than those of MagEIS high while the detrended

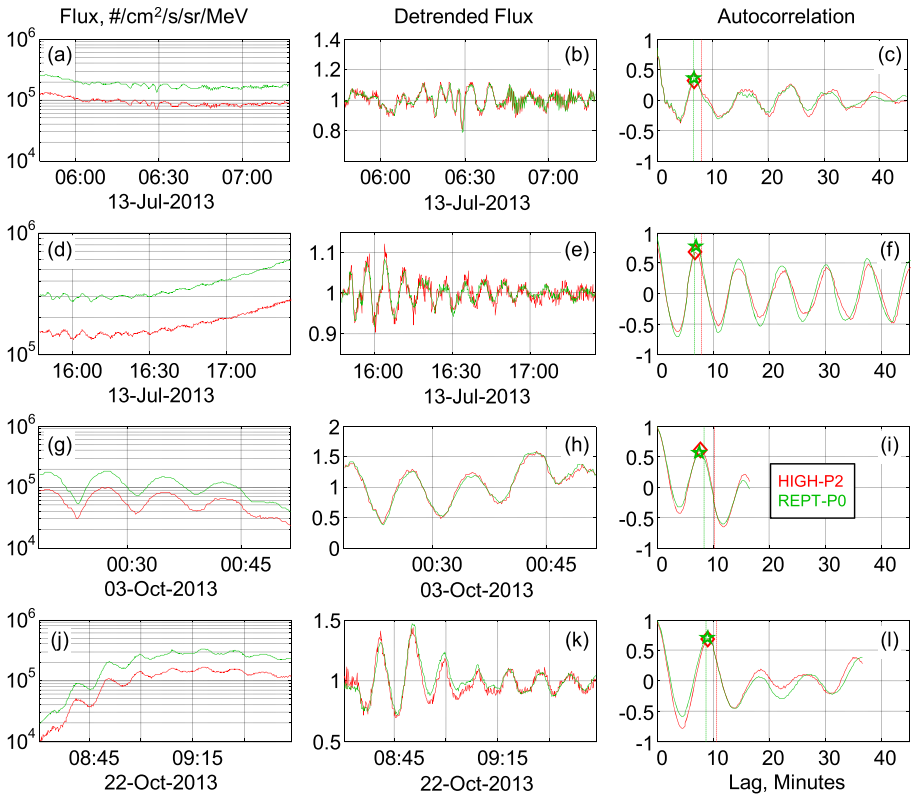

Figure 3. Time series analysis of the MagEIS high P2 channel and the REPT-P0 channel for all four drift echo events. The format is the same as Figure 2.

fluxes and autocorrelations are almost indistinguishable, suggesting these two channels have very similar relative energy response, within a multiplicative scale factor that was removed by detrending. The REPT channel in data release 2 has the bowtie energy range 1.8–2.2 MeV, which is often simply averaged to 2.0 MeV, and the MagEIS channel is labeled 1.6 MeV. Clearly, there is something amiss with these energy assignments. With the drift echo technique, we can perform a quantitative analysis to learn more about the nature of the discrepancy, and we can estimate the effective energy for each channel.

5. Drift Period Analysis

First, we examine channel *TL* ratios. Figure 4 shows the *TL* ratios for all 19 channels for all four events, except for six instances where no drift echo was found. The reference channel is MagEIS medium (M75) P6, nominally measuring 0.743 MeV electrons. We chose this reference channel because the MagEIS medium sensor is simpler than the MagEIS high or REPT sensors, because M75 is more closely aligned with the high unit and with REPT than is the M35 unit, because the nominal energy bandwidth is fairly narrow (about 26% full width at half maximum (FWHM)), and because P6 exhibits drift echoes in all four events. Small symbols give the *TL* ratios for individual events, and larger symbols give the averages over all observed events. We have included 2σ error bars to roughly indicate the 95% confidence on the average. Because we are examining multiple separate events, these error bars account for all the error sources, including data resolution and uncertainty in the autocorrelation.

Using the reference channel, we can compute the expected *TL* ratio for every other channel given its nominal ("release 2") energy. That calculation gives the black trace in Figure 4. We see that quite a few channels have *TL* ratios that fall far from the prediction based on M75-P6. One RBSPICE channel and one MagEIS high are too low, and all three REPT channels and one MagEIS high channel are too high. However, this analysis does not take into account uncertainty in the energy assignment for M75-P6 nor does it actually calculate the expected energy for the other channels. In the next step of our analysis, we will add the rigor needed to

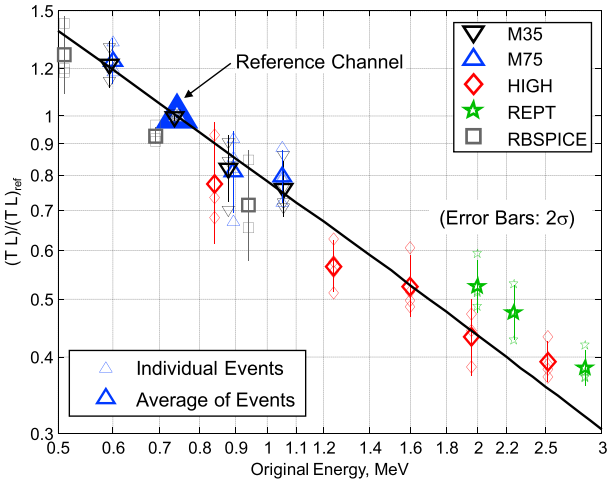

Figure 4. Ratio of drift period (*T*) and *L* shell relative to a reference channel (M75-P6, 0.743 MeV). Small symbols indicate the ratio for individual drift echo events. Medium-sized symbols indicate the average ratio for each channel over all events. Error bars indicate two standard deviations of the average ratio. The large symbol indicates the reference channel. The diagonal line indicates the theoretical prediction based on the reference channel energy.

produce energy estimates with error bars—and we use a technique that can be applied even if the reference channel is not available in every event.

We wish to perform a least squares fit of the log *TL* ratios of all channels to all other channels. We denote the ratio between neighboring channels as

$$r_i = \frac{T_{i+1}L_{i+1}}{T_iL_i} \approx \frac{\left(\frac{E_{i+1}+1}{E_{i+1}(E_{i+1}+2)}\right)}{\left(\frac{E_i+1}{E_i(E_i+2)}\right)}. \quad (8)$$

We denote its natural log as *x*:

$$x_i = \ln r_i. \quad (9)$$

The ratio between any two channels *i* and *j* ($j \geq i$) is then

$$\frac{T_jL_j}{T_iL_i} = \prod_{k=i}^{j-1} r_k, \quad (10)$$

which we can rewrite as a sum by taking the natural log:

$$\ln(T_jL_j) - \ln(T_iL_i) = \sum_{k=i}^{j-1} x_k. \quad (11)$$

Now we can assemble a linear system of equations in the unknowns x_k, with one equation for each unique pair of channels *i,j* in each event. The pairing approach implicitly gives more weight to events involving more channels. If in any event a channel does not exhibit a drift echo, then the pairs involving that channel for that event are simply left out of the system of equations. We have the following:

$$\underline{\underline{A}}\,\vec{x} = \vec{b}\,, \quad (12)$$

$$b_l = \ln(T_jL_j) - \ln(T_iL_i), \quad (13)$$

$$A_{lk} = H(k-i) - H(k-j-1), \quad (14)$$

where *H(n)* is the Heaviside step function, which is zero for $n < 0$ and one otherwise. There are $N_A = 583$ rows in *A* and 18 columns (the length of *x*, one less than the number of energy channels because *x* relates adjacent channels' *TL* ratios). There are $N_T = 70$ observed drift echo periods combined over all four events. N_T is less than the ideal value of $76 = 19 \times 4$ because there were six instances when one of the 19 channels had no echo in one of the four events. Similarly $N_A = 583$ is less than the ideal value of $684 = 4 \times 19 \times (19-1)/2$ because those missing echo periods reduced the number of unique *i,j* pairs.

Because *A* is overdetermined, we solve for *x* in a least squares sense:

$$\vec{x} = \left(\underline{\underline{A}}^T\underline{\underline{A}}\right)^{-1}\underline{\underline{A}}^T\vec{b}\,. \quad (15)$$

We denote the reference channel *j'*, with Energy $E_{j'}$. We can obtain the energy factor for any other channel *i* as

$$\frac{E_i+1}{E_i(E_i+2)} = \frac{E_{j'}+1}{E_{j'}\left(E_{j'}+2\right)} \begin{cases} \exp\sum_{k=i}^{k=j'-1} x_k & i < j' \\ \exp-\sum_{k=j'}^{k=i-1} x_k & i > j' \end{cases}. \quad (16)$$

We can then solve for E_i using the quadratic formula. Appendix A provides more details and error propagation.

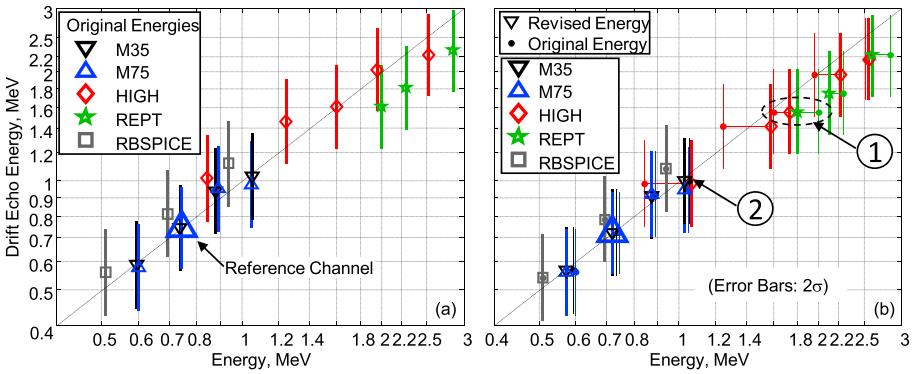

Figure 5. Energy estimates using drift echoes. (a) Energy estimates using the original (release 2) energy channels. The large symbol indicates the reference channel, and the smaller channels indicate the other 18 channels in the analysis. Error bars represent a 95% confidence interval. (b) Energy estimates using the revised energy channels (symbols) with the original energies indicated via filled dots. Marker 1 indicates the convergence of HIGH-P2 and REPT-P0 after revision, as suggested by the synchronized drift echoes in Figures 2q and 3. Marker 2 indicates the convergence of M35-P8, M75-P8, and HIGH-P0 suggested by Figure 2k.

6. Results

Figure 5a shows the results of using the drift periods and the reference channel to determine the energies for all the other channels, comparing these results with the release 2 channel nominal energy assignments. We see now, with 2σ error bars that account for errors in the *TL* ratio and in the reference channel, that three REPT channels have nominal energies that may be too high, while three MagEIS channels are also suspicious (two low, one high). Taking the drift echo energy estimates at face value, we can revisit Figure 1. The red traces indicate the spectra using the drift echo energies (horizontal shifts only). We see that using these energies dramatically reduces the MagEIS high versus REPT discrepancy near 2 MeV (marker A) and nearly completely removes the discrepancy between MagEIS medium and high near 0.9 MeV (marker B). Therefore, a significant part of the flux discrepancy is due to energy channel labeling, not problems with the flux conversion factors. This is not, however, the end of the story.

Our study was conducted simultaneously with various other investigations of the REPT and MagEIS responses to resolve the flux discrepancies. The drift echo analysis suggests that the original (release 2 and prior) REPT energies were too high. This turned out to be at least partly a question of interpretation. The original bowtie analysis [*Baker et al.,* 2012] assigned a lower and upper threshold to each energy channel, which were then averaged to assign a single energy to the channel. Labeling the channel with the arithmetic average of its thresholds is appropriate for a very flat spectrum. However, in the Earth's magnetosphere, electron spectra at multiple MeV are often very steep (see Figure 1).

The REPT differential channel efficiencies were obtained from a Geant4 [*Agostinelli et al.,* 2003] simulation with a complete description of the instrument. These efficiencies were also obtained using both proton and electron beams at accelerator facilities and are in excellent agreement with the Geant4 simulations [*Baker et al.,* 2012]. A bowtie analysis was then applied to these "full" efficiencies to obtain "effective" flux conversion factors and energy labels. For the release 3 data, a new bowtie analysis was recently performed following the method outlined in *Selesnick and Blake* [2000]. This method assigns a single effective energy to each channel rather than an energy bin with a low and high value, as used in *Baker et al.* [2012] for the release 2 and prior data. The revised channel energies are given in contrast to the earlier method (release 2 data, "original") in Table 1. This change resolved a significant part of the flux discrepancy and brought the REPT channel energy labels closer to what the drift echo analysis suggests. It also changed the flux conversion factor (not shown), bringing further improvements to spectral agreement.

MagEIS also completed a full-scale Geant4 simulation of the high unit, accounting for electron scattering inside the magnetic spectrometer and complex interactions between electrons and the silicon detector stack, as well as a realistic magnetic field in the spectrometer. Using the Geant4 results, a new bowtie analysis was also performed using the *Selesnick and Blake* method. Additionally, bowtie analyses were performed for

the low and medium units using results of a physically simpler simulation shown in *Blake et al.* [2013] that neglects scattering and energy deposit physics. The revised channel energies are given in Table 1. We expect further changes to the MagEIS medium channels when they are given the same Geant4 treatment as MagEIS high has received. Given the relatively simpler design of the low and medium sensors, we expect these changes to be smaller than seen in the high unit. The RBSPICE channels have not been revised.

Figure 5b shows the drift echo results versus the revised (bowtie) energies. We can see near marker 1 that in the several cases where MagEIS high and REPT were originally (filled dots) nearly 2σ away from the diagonal, the revised channels move closer to the diagonal. Although the channels near 2 MeV continue to fall below the diagonal, they are all now ordered by drift echo period, suggesting the remaining disagreement lies either in the reference channel or in the simplifying assumptions in the drift echo analysis itself (recall that we accepted a 10% error in order to use spin averages). Near marker 2, we see that the lowest MagEIS high channel now falls very close to the highest MagEIS medium channel. The RBSPICE channels all fall fairly close to the diagonal, even though they were not revised during this study. Overall, it is clear that drift echo analysis provides a valuable tool to help validate the energy assignments, especially the revised ones for MagEIS high and REPT. The updated energies and those derived from the drift echo analysis generally fall within the channel bandwidths, suggesting that the difference is a refinement of the preflight values, as opposed to a correction. We note that some of the original discrepancy arose simply from different approaches to the bowtie analyses used for the MagEIS and REPT instruments.

7. Summary and Conclusion

The drift echo analysis provided a vital clue that inconsistencies in the channel energy labels among MagEIS medium, MagEIS high, and REPT were contributing to the observed flux discrepancies in the release 2 data. An energy labeling inconsistency combined with a steep spectral slope can lead to a significant apparent error in the flux calculated from different sensors, especially when energy channels have relatively large bandwidths. For example, the REPT instrument reports spectra falling as steeply as E^{-10}. In such a situation, even a 25% energy uncertainty (comparable to the channel bandwidth) can lead to nearly a factor of 10 difference in flux.

More generally, the drift echo analysis can supplement other intercalibration techniques that are focused more on flux conversion factors. Drift echoes can potentially tell us more than simply the effective energy for a channel. The echo amplitudes in two channels measuring the same energy should also have the same amplitude, unless one or both flux conversion factors are incorrect or an uncorrected background is present. The decay rate of the envelope of the drift echo tells us about the width of the energy and angle responses of the sensor: wider sensors accept particles with a broader spread of drift periods and therefore exhibit faster decay of the drift echo amplitude.

While it may be tempting to use the drift echo energies outright, we caution that they are best used only as a guide to improving the channel energy response and its interpretation. A more complete understanding of the instrument response is critical for understanding the angular response, the energy bandwidth, the efficiency, and the backgrounds. The drift echo analysis can inform, but not replace, such understanding.

One major limitation of the drift echo method is that it cannot be used at energies for which the large-scale electric field may significantly alter the particle trajectories. However, we envision a related solution for those lower energy particles: drift resonance with ultralow frequency (ULF) waves. During a drift resonance, all energy channels near the resonance will oscillate at the wave frequency, but with an amplitude and phase that depend on the particle energy [see, e.g., *Claudepierre et al.,* 2013]. Because ULF wave periods are typically much shorter than drift periods (i.e., the azimuthal m number of the resonance is much larger than 1), they provide an energy-dependent time domain signature that can be observed on shorter timescales than the drift period. We imagine that one would fit the amplitude-phase relation for the resonance to a set of known channels and then use that relationship to infer the energy and/or flux conversion factors for one or more unknown channels.

Beyond their use for instrument calibration, drift echoes can provide a useful diagnostic of magnetospheric processes. Echoes can arise from dayside solar wind impulses, or nightside impulses associated with dipolarizations. The well-known March 1991 event was caused by a dayside impulse [*Blake et al.,* 1992]. The largest-amplitude event shown in this study was in the early hours of 3 October 2013, associated with

nightside auroral activity during the recovery phase of a moderate magnetic storm. The properties of the drift echoes can shed light on the impulse characteristics [see, e.g., *Gannon et al.,* 2005] and the location of the impulse [see, e.g., *Lanzerotti et al.,* 1967].

Appendix A: Solution for Energy and Error Propagation

We begin by replacing the right side of equation (16) with q_i:

$$\frac{E_i + 1}{E_i(E_i + 2)} = q_i. \tag{A1}$$

We then have a quadratic equation in E_i:

$$q_i E_i^2 + (2q_i - 1)E_i - 1 = 0, \tag{A2}$$

which has only one positive root:

$$E_i = \frac{1}{2q_i} - 1 + \sqrt{1 + \frac{1}{4q_i^2}}. \tag{A3}$$

We begin the error propagation with the error covariance for $\vec{x}$:

$$\mathrm{cov}\left(\delta\vec{x}\right) = \left(\underline{A}^T\underline{A}\right)^{-1}\delta b^2\frac{N_A}{N_T}, \tag{A4}$$

where δb^2 is the mean squared error for b after the fit in (12), The N_A/N_T factor corrects for the overcounting that occurs when the same observed period is used in multiple ratios (rows of A): there are N_T unique drift period observations, but A^TA includes a sum over N_A entries in A. Thus, the N_A/N_T factor ensures that error covariance falls off with $1/N_T$, or δx falls off with $1/\sqrt{N_T}$.

Next we address the dependence of q_i on $\vec{x}$:

$$\frac{\partial q_i}{\partial x_k} = \begin{cases} +q_i & i \le k \le j' - 1 \\ -q_i & j' \le k \le i - 1 \\ 0 & \text{otherwise} \end{cases}. \tag{A5}$$

We also have to consider how q depends on the reference energy $E_{j'}$:

$$\frac{\partial q_i}{\partial E_{j'}} = \frac{q_i}{E_{j'} + 1} - \frac{q_i}{E_{j'}} - \frac{q_i}{E_{j'} + 2}. \tag{A6}$$

Then, the error on δq is as follows:

$$(\delta q_i)^2 = \left(\frac{\partial q_i}{\partial\vec{x}}\right)^T\mathrm{cov}\left(\delta\vec{x}\right)\frac{\partial q_i}{\partial\vec{x}} + \left(\frac{\partial q_i}{\partial E_{j'}}\right)^2\delta E_{j'}^2, \tag{A7}$$

where $\frac{\partial q_i}{\partial\vec{x}}$ is the vector of partial derivatives in (A5). We assume the FWHM energy bandwidth of the reference channel is $2\delta E_{j'}$.

Next, we address the dependence of E_i on q_i:

$$\frac{\partial E_i}{\partial q_i} = \frac{-1}{2q_i^2} - \frac{1}{2q_i^2\sqrt{4q_i^2 + 1}}. \tag{A8}$$

Finally, the error δE_i on E_i is given by:

$$\delta E_i^2 = \left(\frac{\partial E_i}{\partial q_i}\right)^2(\delta q_i)^2. \tag{A9}$$

References

Agostinelli, S., et al. (2003), Geant4—A simulation toolkit, *Nucl. Instrum. Methods A*, *506*(3), 250–303, doi:10.1016/S0168-9002(03)01368-8.

Baker, D. N., et al. (2012), The Relativistic Electron-Proton Telescope (REPT) instrument on board the Radiation Belt Storm Probes (RBSP) spacecraft: Characterization of Earth's radiation belt high-energy particle populations, *Space Sci. Rev.*, *179*(1–4), 337–381, doi:10.1007/s11214-012-9950-9.

Blake, J. B., M. S. Gussenhoven, E. G. Mullen, and R. W. Fillius (1992), Identification of an unexpected space radiation hazard, *IEEE Trans. Nucl. Sci.*, *39*(6), 1761–1764.

Acknowledgments

The MagEIS portion of this work was funded by contract 10-068 from the University of New Hampshire, derived from NASA Van Allen Probes mission funding via RBSP-ECT funding provided by JHU/APL contract 967399. The REPT work was supported by JHU/APL contract 967399 under NASA's prime contract NAS5-01072. Both MagEIS and REPT analyses were supported by the ECT Science Operations Center at Los Alamos National Lab. The RBSPICE instrument was supported by JHU/APL subcontract 937836 to the New Jersey Institute of Technology under NASA prime contract NAS5-01072. The authors also acknowledge useful discussions with our colleagues at The Aerospace Corporation, The Laboratory for Atmospheric and Space Physics at University of Colorado, Boulder, the New Jersey Institute of Technology, and Fundamental Technologies, LLC. ECT data used in the paper are available from www.rbsp-ect.lanl.gov or from the author (paul.obrien@aero.org). RBSPICE data are available from rbspice.ftecs.com.

Michael Balikhin thanks Karel Kudela and P. Daly for their assistance in evaluating this paper.

Blake, J. B., et al. (2013), The Magnetic Electron Ion Spectrometer (MagEIS) instruments aboard the Radiation Belt Storm Probes (RBSP) spacecraft, *Space Sci. Rev.*, *179*(1–4), 383–421, doi:10.1007/s11214-013-9991-8.

Claudepierre, S. G., et al. (2013), Van Allen Probes observation of localized drift resonance between poloidal mode ultra-low frequency waves and 60 keV electrons, *Geophys. Res. Lett.*, *40*, 4491–4497, doi:10.1002/grl.50901.

Friedel, R. H. W., S. Bourdarie, and T. E. Cayton (2005), Intercalibration of magnetospheric energetic electron data, *Space Weather*, *3*, S09B04, doi:10.1029/2005SW000153.

Gannon, J. L., X. Li, and M. Temerin (2005), Parametric study of shock-induced transport and energization of relativistic electrons in the magnetosphere, *J. Geophys. Res.*, *110*, A12206, doi:10.1029/2004JA010679.

Kellerman, A. C., Y. Y. Shprits, D. Kondrashov, D. Subbotin, R. A. Makarevich, E. Donovan, and T. Nagai (2014), Three-dimensional data assimilation and reanalysis of radiation belt electrons: Observations of a four-zone structure using five spacecraft and the VERB code, *J. Geophys. Res. Space Physics*, *119*, 8764–8783, doi:10.1002/2014JA020171.

Lanzerotti, L. J., C. S. Roberts, and W. L. Brown (1967), Temporal variations in the electron flux at synchronous altitudes, *J. Geophys. Res.*, *72*(23), 5893–5902, doi:10.1029/JZ072i023p05893.

Lanzerotti, L. J., C. G. Maclennan, and M. F. Robbins (1971), Proton drift echoes in the magnetosphere, *J. Geophys. Res.*, *76*(1), 259–263, doi:10.1029/JA076i001p00259.

Mitchell, D. G., et al. (2013), Radiation Belt Storm Probes Ion Composition Experiment (RBSPICE), *Space Sci. Rev.*, *179*, doi:10.1007/s11214-013-9995-4.

Olson, W. P., and K. A. Pfitzer (1977), Magnetospheric magnetic field modeling, Annual Scientific Report, Air Force Office of Scientific Research contract F44620-75-C-0033, McDonnell Douglas Astronautics Co., Huntington Bech, Calif.

Sandberg, I., I. A. Daglis, D. Heynderickx, P. Truscott, A. Hands, H. Evans, and P. Nieminen (2014), Development and validation of the electron slot region radiation environment model, *IEEE Trans. Nucl. Sci.*, *61*(4), 1656–1662, doi:10.1109/TNS.2014.2304982.

Schulz, M., and L. J. Lanzerotti (1974), *Physics and Chemistry in Space, Particle Diffusion in the Radiation Belts*, vol. 7, Springer, New York.

Selesnick, R. S., and J. B. Blake (2000), On the source location of radiation belt relativistic electrons, *J. Geophys. Res.*, *105*(A2), 2607–2624, doi:10.1029/1999JA900445.

Spence, H. E., et al. (2013), Science goals and overview of the Radiation Belt Storm Probes (RBSP) Energetic Particle, Composition, and Thermal Plasma (ECT) suite on NASA's Van Allen Probes mission, *Space Sci. Rev.*, *179*(1–4), 311–336, doi:10.1007/s11214-013-0007-5.